Check for updates
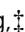
Heterogeneous ZIF-L membranes with improved hydrophilicity and anti-bacterial adhesion for potential application in water treatment†

Qilin Gu, [iD] ‡*[a] Tze Chiang Albert Ng,‡[b] Qiaomei Sun,[c] Abdelnaby Mohamed Kotb Elshahawy,[a] Zhiyang Lyu, [iD] [a] Zeming He,[a] Lei Zhang,[a] How Yong Ng,[b] Kaiyang Zeng [iD] [c] and John Wang*[a]

Although different metal–organic framework (MOF) membranes have been widely studied for gas separation, their application for water treatment is still in its infancy. MOF membranes with improved hydrophilicity and stability are particularly essential for water/wastewater treatment. Herein, we have successfully developed heterogeneous membranes (Zn/Co-ZIF-L) composed of vertically standing leaf-like crystals of Zn-ZIF-L grown *in situ* onto porous ceramic supports, followed by the subsequent heterogeneous growth of Co-ZIF-L. The heterogeneous membranes show improved hydrophilicity (WCA = 13.6 ± 1.6°) and enhanced anti-bacterial adhesion. Significantly, they simultaneously deliver a relative high water flux and much improved anti-bacterial adhesion when compared with the homogeneous membranes (Co-ZIF-L and Zn-ZIF-L). The improvements are attributed to the intrinsic hydrophilic nature of Co-ZIF-L, their epitaxial growth onto Zn-ZIF-L as well as the increased surface roughness. The success of constructing a heterogeneous MOF structure shows an effective strategy to achieve the hydrophilic MOF membranes with considerably enhanced stability for water treatment.

1. Introduction

There has been a constantly increasing demand for clean and usable water for industrial, household and agricultural due to the rapidly on-going industrialization and population growth. Such rapid depletion of freshwater sources necessitates the need to treat and recycle used waters, where membrane treatment is among the best solutions to recover high-quality usable water from both industry and domestic sources. There remains an impetus to explore new emerging advanced membrane materials, especially those durable inorganics and hybrid types.[1–6] Among the recently explored hybrid-type membranes, metal–organic frameworks (MOFs) composed of organic ligands and metal ions are of considerable interest as a class of highly porous materials. Due to the high level of controllable porosity, large surface area and diverse functionalities, MOFs have shown to outperform some of the traditional porous materials such as

zeolite and active carbon, and have been widely studied as adsorbents for purification/separation,[7] hosts for catalysts/ drugs[8] and templates for material synthesis.[9–11] MOF membranes/films with the apparent advantages of high integration and recyclability have been investigated extensively for gas separation,[12–16] while their application potential in water treatment is still at the very early stage of exploration. Most of the known MOFs show poor water stability, which can greatly hamper their application in water and wastewater treatment.[17] Although certain post-treatments with hydrophobic ligands can improve their water stability,[18] the largely hydrophobic surface of MOF membranes generally goes against the requirement of high flux in water treatment. It is thus highly desirable yet challenging to develop MOF membranes with both high hydrophilicity and high stability in water.

Zeolitic imidazolate frameworks (ZIFs) are among the subfamily of MOFs, which are comprised of imidazolate building units within a zeolite-type topology. In 2013, a new type of 2D ZIF with a cushion-shaped cavity between layers and a leaf-shaped morphology, namely ZIF-L was first reported by Wang's group.[19] Due to its porous structure and 2D morphology, ZIF-L has been studied as adsorbents, hosts, templates for gas separation/storage, catalysts, and water purification.[20–23] In our previous work, for example, ZIF-L was utilized as a versatile platform to derive carbon/metal oxide hybrid nanostructures for catalysis applications.[24–26] ZIF-L powders have also been used as fillers to modify polymeric membranes, because of their

[a]*Department of Materials Science and Engineering, National University of Singapore, 117574, Singapore. E-mail: msegq@nus.edu.sg; msewangj@nus.edu.sg*

[b]*Centre for Water Research, Department of Civil and Environmental Engineering, National University of Singapore, 1 Engineering Drive 2, 117576, Singapore*

[c]*Department of Mechanical Engineering, National University of Singapore, 9 Engineering Drive 1, 117576, Singapore*

† Electronic supplementary information (ESI) available. See DOI: 10.1039/c8ra08758j

‡ The authors contributed equally to this work.

intrinsic low zeta potential, relative high hydrophilicity and reduced surface roughness. For example, with the addition of 0.5% ZIF-L, the water flux of polyethersulfone (PES) ultrafiltration membranes was increased by 75% without significantly affecting the molecular weight cutoff (MWCO).[27] Besides, the ordered alignment and the regular apertures of ZIF-L provided ordered water channels for rapid transport of water molecules and a desirable molecular sieving effect. As a result, hybrid-type membranes incorporated with ZIF-L nanosheets showed superior pervaporation performance to that with ZIF-8 nanoparticles.[28] In contrast to the mixing matrix membranes, ZIF membranes with ZIF crystals assembled on robust substrates possess a large effective surface area, improved mechanical stability and high separation performance.[29] For instance, Kang and coworkers[30] reported the growth of ZIF-L crystals on porous α-Al$_2$O$_3$ supports, and the as-obtained membranes showed great potential in dye waste-water purification by the adsorption of dye molecules in aqueous solution.

Compared with the traditional filtration membranes, membrane bioreactors (MBRs) with the integration of biological treatment have emerged as one of the most promising water treatment technologies. The membrane surface for MBRs needs to be hydrophilic and anti-bacterial adhesion in order to inhibit the formation of biofilms. In this connection, porous ZIF-L contains a large number of metal ions showing great potential for anti-bacterial activity.[31] Based on the literature,[32] it is understood that Co-based ZIF-L (Co-ZIF-L) membranes possess better anti-bacterial adhesion capability than Zn-based ZIF-L (Zn-ZIF-L) membranes, and would be more attractive for water purification. However, due to the extremely high reactivity between Co ions and 2-methylimidazole, the heterogeneous nucleation of Co-ZIF-L on substrates is rather difficult. Besides, the poor Co-ZIF-L developed on the substrate would dissolve easily once in contact with water. As a result, only Zn-ZIF-L based membranes have been studied for water purification,[27,30] while Co-based ZIF-L membranes have never been reported.

In this work, a new type of heterogeneous membranes (Co-ZIF-L on Zn-ZIF-L, denoted as Zn/Co-ZIF-L hereafter) composed of vertical standing leaf-like crystals with anti-bacterial adhesion capability, potentially for MBR application, is explored for the first time. The preparation process involves the *in situ* growth of Zn-ZIF-L membranes on porous Al$_2$O$_3$ supports, followed by the subsequent heterogeneous growth of Co-ZIF-L at room temperature. The present study demonstrates the following advantages of the new heterogeneous membranes: (a) benefiting from the structural similarity, Zn-ZIF-L as an interlayer facilitates the growth of Co-ZIF-L crystals; (b) the heterogeneous growth of Co-ZIF-L onto Zn-ZIF-L can effectively modify the stability when compared with pure Co-ZIF-L membranes, (c) Zn/Co-ZIF-L enhances the surface hydrophilicity, thus increasing water permeability; and (d) the addition of Co-ZIF-L on the membrane surface will increase anti-bacterial adhesion. These advantages can enable the potential application of Zn/Co-ZIF-L heterogeneous membranes in water and wastewater treatment.

2. Results and discussion

2.1. Membrane preparation and structural characterization

Given that the dimensions of ZIF-L crystals are several micrometers in width and length,[24] ceramic supports with an average pore size of $\sim$2 μm (Fig. S1†) were selected for the growth of ZIF-L membranes. The relatively large pore size of the supports would benefit the effective water permeation with low transport resistance.[33] The preparation process of Zn/Co-ZIF-L heterogeneous membranes is schematically illustrated in Fig. 1. In the process, commercially available porous α-Al$_2$O$_3$ ceramic supports after pretreatment were vertically placed into the precursor solution and kept standing at room temperature for 4 h. Followed by repeated washing using water and overnight drying at 60 °C, homogeneous Zn-ZIF-L (or Co-ZIF-L) membranes were grown on the ceramic support (Fig. 1b). Heterogeneous membranes (Zn/Co-ZIF-L) were prepared by the subsequent growth of Co-ZIF-L onto the Zn-ZIF-L membranes with a similar process, except for the substitution of Zn(NO$_3$)$_2$·6H$_2$O by Co(NO$_3$)$_2$·6H$_2$O (Fig. 1c). As a result, both homogeneous membranes (Zn-ZIF-L and Co-ZIF-L) and heterogeneous membranes (Zn/Co-ZIF-L) were prepared by the facile and energy-efficient process.

Precursors provide the sources for ZIF-L growth, and the resultant microstructure of the selective layer is thus closely related to the characteristics (such as concentration) of the precursors and the duration of growth.[34] For example, Zn-ZIF-L membranes prepared with 1.0 mmol L^{-1} Zn(NO$_3$)$_2$ are composed of poorly developed crystals and the coverage is patchy, as the pores from the substrate layer could be observed (Fig. S2a and b†). However, with an increased precursor concentration of 2.0 mmol L^{-1}, a homogeneous layer with leaf-like Zn-ZIF-L crystals vertically standing on the ceramic supports are observed. These crystals, with an average thickness of $\sim$200 nm, are well-developed and cross-linked (Fig. S2c and d,† and 2). Both the morphology and size of Zn-ZIF-L crystals are consistent with those of previous reports.[35] When the reaction time is shortened to less than 4 h, the thin ZIF-L crystals are not uniform, and the Al$_2$O$_3$ grains on the ceramic substrate surfaces are exposed (Fig. S3†). EDS results show the existence of Zn ions on the substrates after 40 min (Fig. S3b†), confirming the preferential bonding of Zn ions on the hydrophilic supports with hydroxyl groups (Fig. 1a). Compared with the previous work,[29] where O$_2$ plasma treatment was used to increase the hydrophilicity of the supports (such as glass and nylon microfibers), the intrinsic hydrophilic characteristic of Al$_2$O$_3$ supports in this work simplified the preparation process. Note that certain small ZIF-L grains are found coated on the inner walls of surface pores and their further growth would increase the coverage and improve the selectivity of the membranes (Fig. S4†).[36]

SEM images (Fig. 2a–c) show that the average thickness of the Co-ZIF-L and Zn/Co-ZIF-L crystals is comparable to that of Zn-ZIF-L ($\sim$200 nm). In addition, the thickness of the ZIF-L membranes was determined by examination of the cross-section using SEM. Prior to the SEM study, each sample was

Fig. 1 Schematic illustration of the preparation process and microstructure of homogeneous (Co-ZIF-L, Zn-ZIF-L) and heterogeneous (Co-ZIF-L on Zn-ZIF-L, denoted as Zn/Co-ZIF-L) ZIF-L membranes on porous ceramic supports. (a) Macroporous Al_2O_3 ceramic supports with surface hydroxyl groups, which endow their intrinsic hydrophilicity. (b) Zn-ZIF-L membranes formed by the growth of Zn-ZIF-L on the surface of ceramic supports through the reaction of zinc nitrate and 2-methylimidazole at room temperature for 4 h. Similarly, Co-ZIF-L membranes can be obtained by replacing zinc nitrate with cobalt nitrate. (c) Heterogeneous Zn/Co-ZIF-L membranes prepared by the subsequent growth of Co-ZIF-L onto Zn-ZIF-L membranes. In addition, the potential chemical bonds at the interface are illustrated in the enlarged views.

fresh cut. However, Co-ZIF-L crystals cannot be clearly identified from the cross-sectional SEM images (Fig. 2d), because the stability of these ZIF crystals is so poor that they would dissolve during the water-assisted cutting process. Instead, fusion-like substances derived from the dissolution of Co-ZIF-L crystals, which is further demonstrated to be $Co(OH)_2$ (JCPDS no. 51-1731, Fig. S5†), cover on the surface of the ceramic supports (Fig. 2d). In contrast, it is clearly observed that Zn-ZIF-L crystals are largely vertically grown with a thickness of approximately 6 μm, and the subsequent growth of the Co-ZIF-L layer increases the thickness to 15 μm (Fig. 2e and f). To properly examine the cross-section of Co-ZIF-L membranes using SEM, samples were then cut without the use of cooling water. As shown in Fig. S6,† the density of Co-ZIF-L membrane is slightly lower than that of Zn-ZIF-L membrane. Elemental distribution along individual leaf-like crystals of Zn/Co-ZIF-L membranes presents a sharp change between Co and Zn elements (Fig. 2g–i). The increment of membrane thickness and variation of element distribution both confirm the heterogeneous growth behavior of Co-ZIF-L on Zn-ZIF-L crystals. The growth of Co-ZIF-L on Zn-ZIF-L is regarded as the epitaxial secondary growth. Different from the recent observation of hierarchical ZIF-L nanostructures formed by the secondary growth process,[29,37] the ZIF-L crystals appear to be leaf-like in our work, raising from the numerous nucleation

sites of the hydrophilic supports, which confine the growth in largely vertical direction to the supports.

ZIF-L is known to be a metastable phase which would transform to ZIF-67 (Co-ZIF-L) or ZIF-8 (Zn-ZIF-L). Specifically, the transformation of Co-ZIF-L to ZIF-67 was observed at room temperature in water,[38] while the transition from Zn-ZIF-L to ZIF-8 took place at elevated temperature (60 °C).[39] The microstructure evolution of these ZIF-L membranes in water at room temperature was then comparably studied to evaluate their stability in water. As shown in Fig. S7(a),† the poorly developed Co-ZIF-L membrane would disappear from the substrate after 30 min; while the Zn/Co-ZIF-L membranes can withstand being submerged in water for more than 60 min. This indicates the improved stability of the heterogeneous Zn/Co-ZIF-L membranes, resulting from the relatively strong bonding Co-ZIF-L onto the Zn-ZIF-L compared with the direct heterogeneous growth on ceramic supports (Fig. 1c). It is known that there are some hydroxyl groups (–OH) on the surface of the ceramic supports, and the Zn ions would chemically bond accordingly as the reactive sites for the vertical growth of Zn-ZIF-L (Fig. S3†), as the metal ions are the terminal atoms for ZIF-L.[40] It is thus inferred that the Zn–O bonds would be formed between the ceramic support and Zn-ZIF-L membrane, as illustrated in Fig. 1. While Co ions have relatively high reactivity with 2-MIM, and the heterogeneous growth on the ceramic
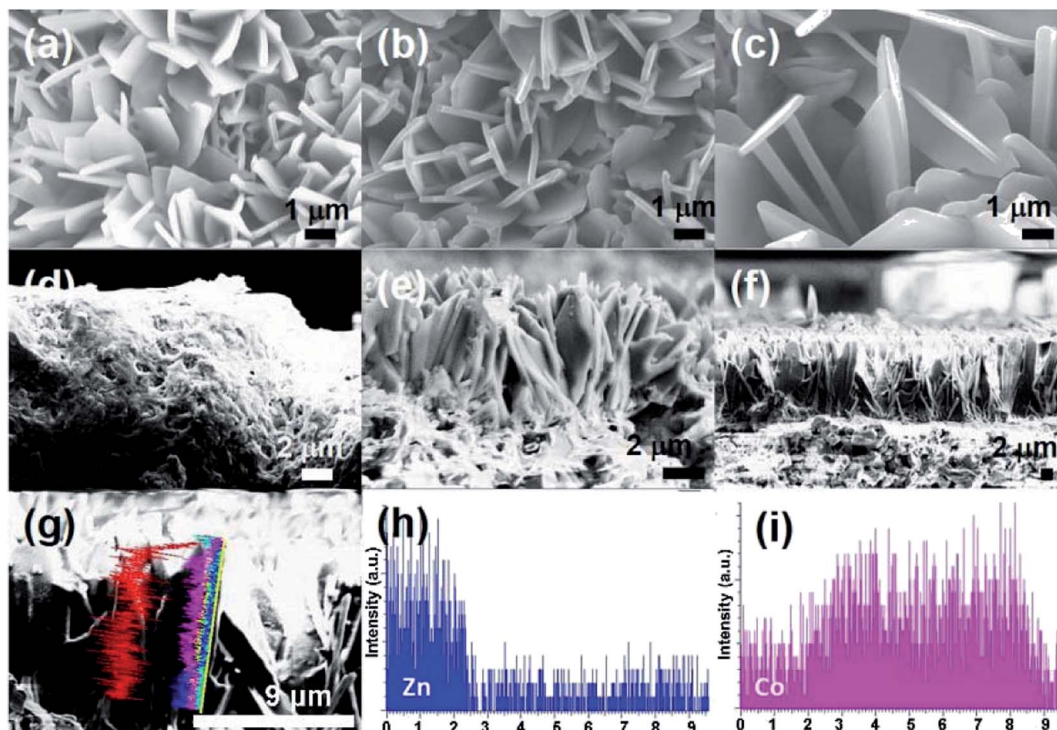
Fig. 2 Microstructure and elemental distribution of ZIF-L membranes: (a and d) Co-ZIF-L, (b and e) Zn-ZIF-L, (c and f) Zn/Co-ZIF-L, (g–i) element distributions of Zn and Co.

support is quite poor. As a result, Co-ZIF-L and Zn-ZIF-L membranes show a slight difference in density on the ceramic support, as shown in Fig. 2a and b. To confirm the chemical bond between the ceramic supports and Zn-ZIF-L membranes, the interfacial chemistry was checked by XPS study. As shown in the high-resolution O 1s XPS spectra (Fig. S8†), there exists an

additional peak at 528.88 eV attributing to Zn–O bonds between the ZIF-L membranes and ceramic support. After stirring in water for 120 min (Fig. S7†), both Co-ZIF-L and Zn-ZIF-L membranes are destroyed, and only some fragments remain in the macropores of the supports. In contrast, the surface of Zn/Co-ZIF-L membranes remains uniformly covered by the Zn/

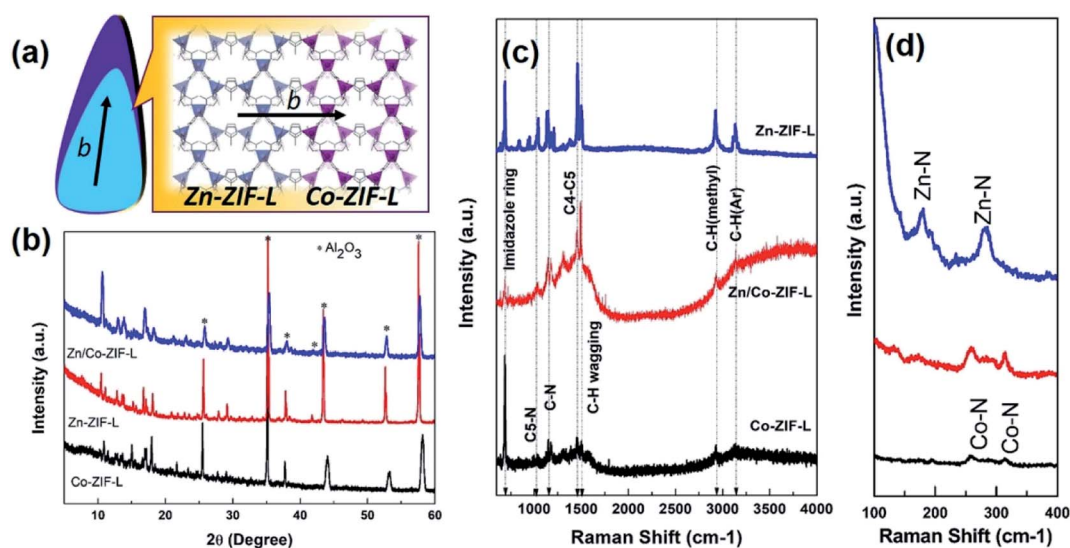Fig. 3 Structural characterization of ZIF-L membranes. (a) Schematic illustration of the crystal structure for the heterogeneous growth of Co-ZIF-L on Zn-ZIF-L along b-axis. (b) XRD patterns of homogeneous membranes (Zn-ZIF-L and Co-ZIF-L) and heterogeneous membranes (Zn/Co-ZIF-L) grown on porous ceramic supports. (c and d) Raman spectra of Zn-ZIF-L, Co-ZIF-L and Zn/Co-ZIF-L samples collected from the corresponding membranes.
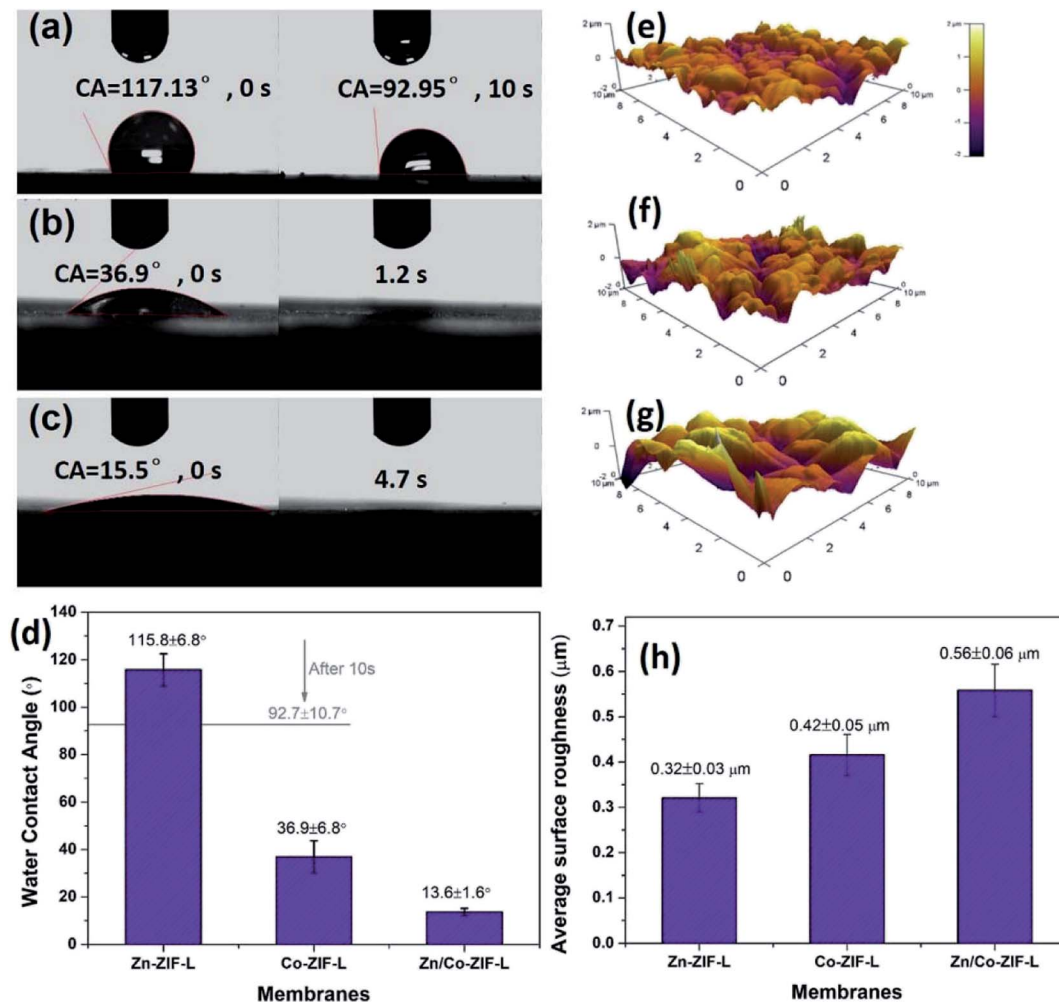
Fig. 4 Surface characteristics of ZIF-L membranes. Representative water contact angle of (a) Zn-ZIF-L, (b) Co-ZIF-L, (c) Zn/Co-ZIF-L, and (d) summarized histogram of the water contact angle for ZIF-L membranes. Surface topography of ZIF-L membranes: (e) Zn-ZIF-L, (f) Co-ZIF-L, (g) Zn/Co-ZIF-L in the area of 10 μm × 10 μm, and (h) the average surface roughness of ZIF-L membranes.

Co-ZIF-L derived nanosheets (Fig. S9†). Such laminated structures are well-preserved after 24 h (Fig. S10†). These results indicate that the Zn/Co-ZIF-L heterogeneous membranes show better water stability than that of Co-ZIF-L and Zn-ZIF-L membranes, and also the derived laminated membranes would continue to serve as the designed functional layers. During the water stability test, there hardly observed free-standing powders in the solution, suggesting that the unsatisfied long-term stability of the membranes was not caused by the interfacial attachment, but mainly related to the intrinsic chemical stability of the ZIF-L crystals. Moreover, these experimental observations suggest that particular attention should be paid to the microstructures of ZIF-L membranes after filtration, which has not been properly characterized previously.[30]

In ZIF-L, the 2D layer network along the *ab* plane is composed of interconnected hexagons and parallelograms formed by different Zn ions, and these layers are then stacked along the *c* direction.[20,40] As illustrated in Fig. 3a, the heterogeneous growth of Co-ZIF-L on Zn-ZIF-L is along the *b*-axis. The similar crystalline structure ensures the heterogeneous growth

of Co-ZIF-L onto Zn-ZIF-L. As a result, both XRD patterns (Fig. 3b) and Raman spectra (Fig. 3c) of Zn/Co-ZIF-L membranes are similar to those of Zn-ZIF-L and Co-ZIF-L membranes. The degree of crystallinity of Co-ZIF-L membranes is quite poor, compared to that of Zn/Co-ZIF-L and Zn-ZIF-L membranes, since the heterogeneous growth of Co-ZIF-L on supports is rather difficult.[41] The signature of C–H (Ar), C–H (methyl), C–N and imidazole ring located at around 3134 cm^{-1}, 2924 cm^{-1}, 1148 cm^{-1} and 689 cm^{-1}, respectively can all be identified in the Zn/Co-ZIF-L, Zn-ZIF-L and Co-ZIF-L membranes.[42] The locally structural difference between Co-ZIF-L and Zn-ZIF-L is reflected by Raman shift of metal–N bond (Fig. 3d), since the length of Zn–N bond is shorter than that Co–N bond.[43] The stronger Zn–N bond can contribute to the higher stability of heterogeneous membranes.

2.2. Surface characteristics

MOF-based heterogeneous structures including core–shell structure[44,45] and layer-by-layer structure[41,46] have previously
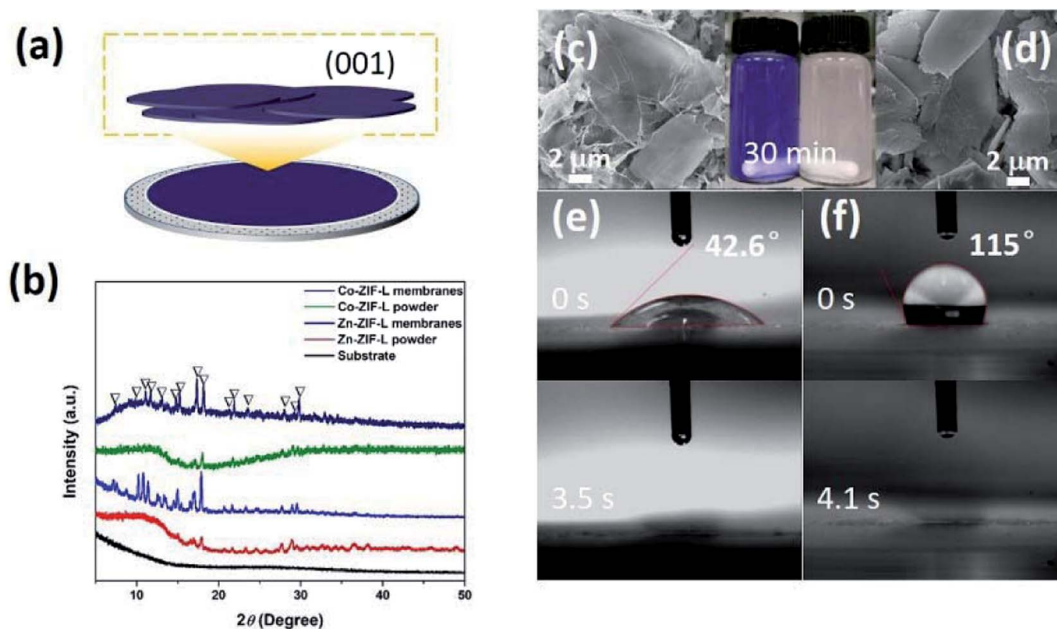
Fig. 5 ZIF–L membranes prepared by the deposition of leaf-like ZIF-L powders on filters by vacuum filtration: (a) illustration of the microstructure of ZIF–L membranes, where the leaf-like ZIF-L powders are coated on commercial polymeric support with the *c*-axis orientation; (b) XRD pattern of the deposited ZIF-L membranes, random powders and the commercial substrate; SEM image of the deposited (c) Co-ZIF-L membranes and (d) Zn-ZIF-L membranes, the inset shows photograph of the dispersion of Co-ZIF-L (purple) and Zn-ZIF-L (white) powders in water; water contact angle of the deposited (e) Co-ZIF-L and (f) Zn-ZIF-L membranes.
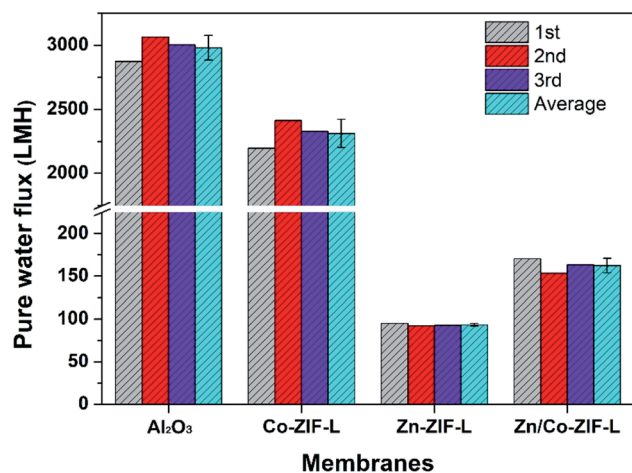

Fig. 6 Pure water flux of the membranes.

been prepared, and the MOF composites thus-formed show improved separation performance as a result of the engineered pore structure. Specific MOFs can be selected as an interlayer for the growth of target MOFs in terms of the difference in microstructures and chemical characteristics.[47] Given the successful formation of the Zn/Co-ZIF-L heterogeneous membranes, we have explored their stability and potential applications for water and wastewater treatment.

Zn-ZIF-L membranes show a rather hydrophobic surface with WCA of 117°, and after 10 s, the WCA slightly reduces to 92.95° (Fig. 4a). In contrast, the surface of Co-ZIF-L membranes

is much more hydrophilic with WCA of 36.9°, and the water droplet can be infiltrated rapidly (~1.2 s) (Fig. 4b). Notably, a superhydrophilic surface (WCA = 15.5°) is obtained for the Zn/Co-ZIF-L membranes (Fig. 4c). It is known that the wettability of the membrane surface is comprehensively determined by the chemical composition, surface roughness and surface energy.[48] Membrane surfaces with improved hydrophilicity are beneficial for water permeation and anti-fouling properties since most foulants are hydrophobic. As characterized by AFM (Fig. 4e–h), the surface roughness of Zn/Co-ZIF-L membranes ($R_a = 0.56 \pm 0.06$ μm) is increased compared with that of Zn-ZIF-L ($R_a = 0.32 \pm 0.05$ μm) and Co-ZIF-L ($R_a = 0.42 \pm 0.05$ μm) homogeneous membranes.

Through the deposition of ZIF-L powders onto commercial ceramic membranes, the intrinsic wettability of the ZIF-L crystals on (001) facets was characterized (Fig. 5a). XRD patterns (Fig. 5b) and SEM images (Fig. 5c and d) demonstrate the horizontal orientation of the leaf-like ZIF-L crystals in the membranes. XRD patterns of ZIF-L powders deposited on the substrate show a relative high intensity. In contrast, the XRD pattern of the ZIF-L powders is not very sharp, because of the random orientation of the ZIF-L powders and rough surface. By comparison of the random powders with the deposited membranes, the main peaks are consistent with each other, both of which also agree with the previous work.[37] As shown in Fig. 5e and f, the WCA for Zn-ZIF-L and Co-ZIF-L membranes is 115° and 42.6°, respectively. The hydrophilicity of Co-ZIF-L crystals is therefore much better than that of Zn-ZIF-L crystals. Besides, the hydrophilicity is further improved for the
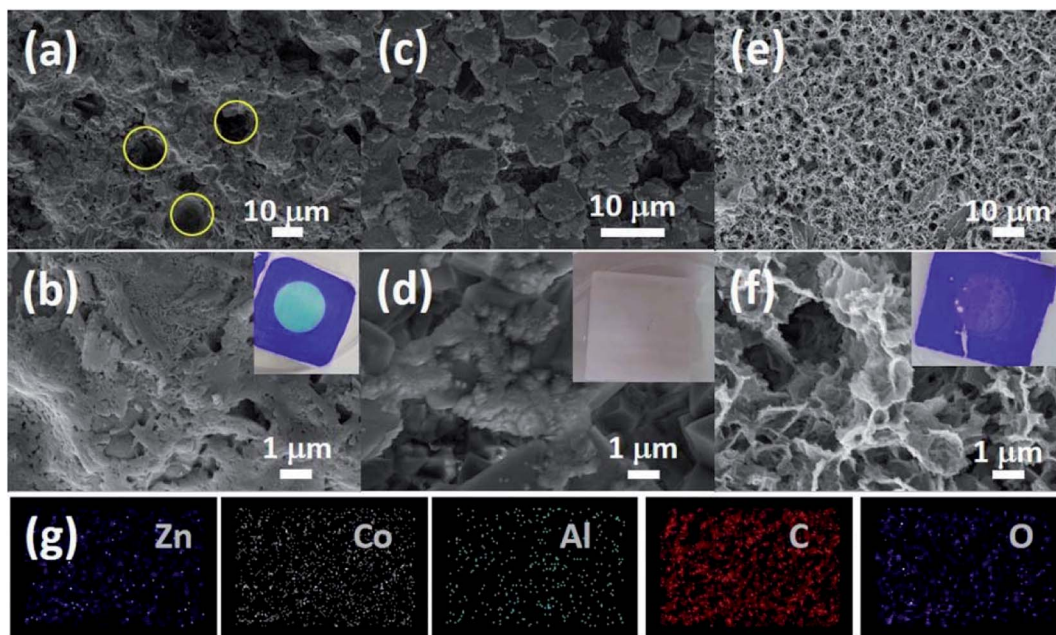
Fig. 7 Surface SEM images of ZIF-L membranes after pure water flux test: (a and b) Co-ZIF-L, (c and d) Zn-ZIF-L, (e and f) Zn/Co-ZIF-L. The insets show the corresponding photographs of samples after water flux test, where the test was conducted on a circular area with a diameter of 16 mm. (g) The elemental distribution of the testing area in the Zn/Co-ZIF-L membrane after the water flux test.
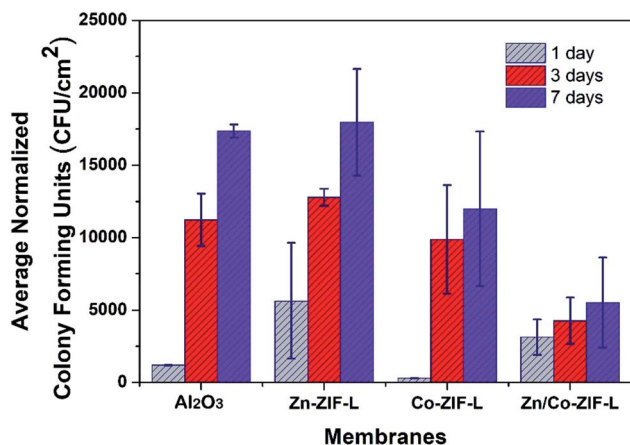

Fig. 8 Average normalized colony forming units (CFU) of the membranes after 1, 3 and 7 days.

vertically grown ZIF-L membranes as a result of the unique structure with increased surface roughness.[49]

2.3. Pure water flux

To evaluate the potential of ZIF-L membranes for water and wastewater treatment (*e.g.* MBR, which is a widely investigated technology for water treatment with the combination of filtration membranes and biological treatment[50]), their pure water flux and anti-bacterial adhesion properties were measured. As shown in Fig. 6, the water flux of Co-ZIF-L reaches a value of 2312.5 LMH, approximately 78% of the pristine Al_2O_3 substrates (2979.17 LMH), while Zn-ZIF-L membranes deliver a pure water

flux of ~93.33 LMH. The observed significant difference mainly originates from their different stability. According to the available literature,[34] and the observed microstructure of Co-ZIF-L after the dead-end filtration (Fig. 7a and b), Co-ZIF-L appears to be rapidly degraded, and the derived segments can hardly prevent the water transport. Compared to homogeneous Zn-ZIF-L membranes, the water flux of heterogeneous Zn/Co-ZIF-L membranes is nearly doubled (162.5 LMH *vs.* 93.33 LMH). The average pore size of the as-prepared heterogeneous membranes is evaluated to be ~44.3 nm by nitrogen adsorption–desorption isotherms, which are mainly situated at the grain boundaries/junctions of ZIF-L crystals (Fig. 2f). Notably, the pure water flux of Zn-ZIF-L membranes is quite stable as indicated by the narrow error bar, suggesting the improved stability in water. These results indicate that Zn ions are required for better stability in water, and the inclusion of Co ions to create the heterogeneous membrane with increased hydrophilicity would improve the water transport.

After the water flux test, the selective layer of homogeneous membranes (Zn-ZIF-L and Co-ZIF-L) almost disappear, and the macropores on the substrates could be observed (Fig. 7a–d). In particular, as shown in Fig. 7d, some small particles aggregate together and block the surface pore of the supports. This would also contribute the observed reduction in pure water flux of Zn-ZF-L membranes. For Zn/Co-ZIF-L membranes, the nanosheets are observed to uniformly cover the substrates, which are composed of Zn, Co, C, and O elements (Fig. 7g). The insets in Fig. 7b, d and f show the photographs of membranes after water flux test. The color of Co-ZIF-L membranes changes to light green, while the Zn/Co-ZIF-L remains purple as the prepared.

Thus, it is proved that Zn/Co-ZIF-L heterogeneous membranes show much-improved water stability.

The time-dependent pure water flux in extended duration is also provided as an alternative to evaluate the stability of the heterogeneous Zn/Co-ZIF-L membranes, as shown in Fig. S11.† At first, the heterogeneous Zn/Co-ZIF-L membranes show the highest water flux, due to the improved hydrophilicity and surface roughness. A gradual decline in pure water flux with time is resulted from the dislodged ZIF-L crystals that block some of the membrane pores. With further prolonging in time, the pure water flux started to increase, indicating that some of the selective layers had been destroyed. As shown in Fig. S11,† the heterogeneous Zn/Co-ZIF-L membranes exhibit a relatively longer lifetime compared to others, suggesting the improved stability of the heterogeneous membranes.

2.4. Anti-bacterial adhesion

To evaluate the activity against bacterial adhesion, ZIF-L and commercial membranes were submerged in a sequencing batch reactor treating domestic used waster under static conditions (no filtration). The biofilm mass that formed on the surfaces of the membranes were measured by determining the number of live bacteria through the determination of colony forming units (CFU).[51]

Results in Fig. 8 show that the Zn-ZIF-L membranes are unable to inhibit bacterial adhesion on the membrane surface at all sampled time points. In contrast, the 7 day biofilm growth has been clearly inhibited for both Co-ZIF-L and Zn/Co-ZIF-L membranes. Co-ZIF-L membranes show particularly good inhabitation of bacterial adhesion after 1 day. However, this effect is markedly reduced as the experiment progressed. The phenomenon could be explained by the poor stability of Co-ZIF-L.[34] SEM images of the membrane surface after growth of bacterial are provided in Fig. S12.† It is observed that Co-ZIF-L crystals can be hardly identified, and there presents a molten state similar to Fig. 2d. In contrast, the basic framework of ZIF-L crystals is retained in the Zn-ZIF-L and Zn/Co-ZIF-L membranes. Bacteria cells, after fixation, can be easily observed on Zn-ZIF-L membranes, while traces of these cells could hardly be detected on the Zn/Co-ZIF-L surface. Despite having a rougher surface than other membranes, Zn/Co-ZIF-L membranes display the highest activity against anti-bacterial adhesion among the membranes tested with a reduction of more than 50% compared to the commercial ceramic membranes. It is postulated that, in addition to the effect of Co ions,[32] the nanostructures of the ZIF-L layer prevent bacterial adhesion by reducing the adhesion surface area.[52] Therefore, Zn/Co-ZIF-L membranes possess the best anti-bacterial adhesion in terms of growth inhabitation and stability.

Based on the above results, the formed Zn/Co-ZIF-L heterogeneous membranes show much-improved hydrophilicity and water stability compared with homogeneous ZIF-L membranes. In combination with enhanced anti-bacterial adhesion performance, the as-prepared Zn/Co-ZIF-L membranes are demonstrated to be potential for MBR applications. Besides, post-modification with hydrophobic ligands (i.e. benzimidazole)

was conducted,[53] and water stability of modified membranes can be improved as expected (Fig. S13†). However, the super-hydrophobic surface (WCA = 129°) results in a dramatic reduction of water flux (59.58 ± 22.08 LMH). In comparison, the construction of heterogeneous membranes is a promising strategy to simultaneously improve the stability and hydrophilicity of ZIF-L membranes.

3. Conclusion

In this work, heterogeneous Zn/Co-ZIF-L membranes were prepared on commercial porous ceramic supports. The preparation process involved an *in situ* growth of Zn-ZIF-L and the subsequent heterogeneous growth of Co-ZIF-L. The heterogeneous growth of Co-ZIF-L onto the Zn-ZIF-L is demonstrated by the increase in membrane thickness (from 6 μm to 15 μm) and the obvious composition variation along the thickness direction. Due to the hydrophilic nature of Co-ZIF-L and its increased surface roughness, the hydrophilicity of the heterogeneous membranes is greatly improved. Benefiting from the purposely-controlled heterogeneous growth of hydrophilic Co-ZIF-L, the heterogeneous Zn/Co-ZIF-L membranes not only show improved anti-bacterial adhesion performance but also deliver relative high and stable water flux (162.5 LMH). Post-modification with hydrophobic ligands could further improve the stability of heterogeneous membranes, but the pure water flux would be decreased, as a result of the hydrophobic surface. Thus, we conclude that the heterogeneous growth and microstructure regulation are promising approaches to improve the stability of ZIF as well as other MOF membranes without sacrificing hydrophilicity, in order to extend their potential in water and wastewater treatment.

4. Experimental section

4.1. Chemicals and materials

Chemicals including 2-methylimidazole ($C_4H_6N_2$, 99%), cobalt nitrate hexahydrate ($Co(NO_3)_3 \cdot 6H_2O$, 98%), and zinc nitrate hexahydrate ($Zn(NO_3)_2 \cdot 6H_2O$, 99%) were purchased from Sigma-Aldrich and used as received without further purification. Commercial porous ceramic substrates (α-Al_2O_3, pore size: ~100 nm) were cut into pieces of 2.5 × 2.5 cm² followed by slight polishing, ultrasonic treatment in water and then drying at 100 °C for 1 h. In order to avoid the growth of MOF crystals inside the channels, all edges of the porous ceramic substrates were covered by plastic tape.

4.2. Preparation of ZIF-L homogenous membranes

The preparation process from our previous work was used with minor modifications.[25] Zinc nitrate hexahydrate (0.5820 g) and 2-methylimidazole (1.3000 g) were each dissolved in 40 mL of deionized (DI) water. After stirring for 10 min, the zinc nitrate solutions were added into the 2-methylimidazole solution. Right after mixing the two solutions, commercial ceramic supports with the lateral side sealed by plastic tape were vertically placed into the mixture and kept for 4 h at room

temperature. After being washed with DI water and drying in an oven at 60 °C, samples including Zn-ZIF-L nanostructure grown on alumina ceramics and the Zn-ZIF-L powders were obtained. Similarly, Co-ZIF-L nanostructure grown on alumina ceramics and Co-ZIF-L powders were prepared by replacing the zinc nitrate with an equal molar amount of cobalt nitrate hexahydrate.

4.3. Preparation of Zn/Co-ZIF-L heterogeneous membranes

Cobalt nitrate (0.5930 g) and 2-methylimidazole (1.3000 g) were each dissolved into 40 mL deionized (DI) water. After stirring for 10 min, the zinc nitrate solutions were then added into the 2-methylimidazole solution. Right after mixing the two solutions, the as-prepared Zn-ZIF-L membranes with the lateral side sealed by plastic tape were vertically placed into the mixture and kept for 4 h at room temperature. After being washed with DI water and drying in the oven at 60 °C, samples with Co-ZIF-L nanostructure grown on Zn-ZIF-L membranes were obtained.

4.4. Preparation of *c*-oriented ZIF-L membranes

10 mg of Co-ZIF-L (or Zn-ZIF-L) powders were first dispersed in 20 mL of DI water followed by moderate stirring at 200 rpm for 30 min. The *c*-oriented Co-ZIF-L (or Zn-ZIF-L) membranes were then deposited on filters by vacuum filtration (600 mm Hg, 15 min). The as-prepared membranes were then dried at 60 °C for 30 min for further characterization.

4.5. Surface modification

In order to improve the water stability of as-prepared ZIF-L membranes, a post-ligand-exchange reaction was conducted according to the previous work.[53] In detail, a chemical solution was made by dissolving benzimidazole (0.5 g) and sodium acetate (0.35 g) in methanol (50 mL). The above prepared ZIF-L membranes were vertically placed into the solution and kept standing at room temperature for 24 h. The modified membranes were then washed with methanol for 2 times to completely remove any free 2-methylimidazole and free benzimidazole. The products were then dried in an oven at 100 °C for 24 h.

4.6. Characterization

The morphology was determined using an SEM (SUPRA 40 ZEISS, Germany). The samples were pretreated by gold sputtering (30 s, 20 mA) prior to the measurement. XRD patterns were acquired using an X-ray powder diffraction Bruker D8 diffractometer operating at 40 kV and 40 mA using Cu K radiation (0.15406 nm). Raman spectra were collected on a Thermo Scientific DXR Raman microscope with a 514 nm excitation. The water contact angle was measured with a VCA Optima surface analysis system (Advanced Surface Technology, Billerica, MA) using a water droplet (1.5 μL) as an indicator. AFM was performed using a Molecular Force Probe 3D Controller (Asylum Research-MFP 3D) to measure the surface roughness. Each sample was measured at least three times. Nitrogen adsorption–desorption isotherms of the membranes were measured on

a Micromeritics ASAP 2020 at 77 K. Before each measurement, samples were degassed at 100 °C for 4 h, and the average pore size was evaluated using the BJH desorption dV/dw pore volume.

4.7. Anti-bacterial adhesion measurement

Membrane samples were submerged in a Sequencing Batch Reactor (SBR) and sampled after 1, 3 and 7 d. Return activated sludge from a water reclamation plant treating domestic and light industry wastewater was used as the seed in the SBR. The operating conditions were maintained at 6 h hydraulic retention time and 15 d solids retention time to simulate operating conditions in an MBR throughout the test. The SBR was operated continuously for 3 months to acclimatize the sludge before the test began. Primary effluent from a used water treatment plant in Singapore served as the substrate for the sludge. The membrane surface to be taken for cell count was washed with 1 mL of sdH$_2$O for every square centimeter of membrane surface thrice. Then, the biofilm was detached from the membrane surface by vortexing the membrane in sdH$_2$O for 5 min. The strongly adhered bacteria were gently scraped from the surface with a sterile pick and mixed in the sdH$_2$O. The resulting suspension was diluted to an appropriate amount and spread onto the surface of prepared LB-agar plates. The plates were then incubated at 30 °C for one day before colonies were counted. The presence of each colony represented one live cell from the biofilm on the membrane surface and is reported as colony forming units (CFU).

4.8. Water flux

Water permeation was determined using a dead-end filtration setup. Pure water used for the filtration was prepared by passing MilliQ water through a 0.02 μm filter to ensure the removal of colloidal particles, which would interfere in the filtration process. Before filtration, the cleaned membranes were fully saturated with pure water in a pressurized tank at −0.095 MPa for 5 min. The pure water flux was evaluated with a filtration area of the diameter of $\phi = 16$ mm and at a pressure of 100 kPa. The permeate water was collected and weighed by a precision balance. For each sample, the test was repeated three times.

Conflicts of interest

The authors declare no conflict of interest.

Acknowledgements

References

1 K. H. Thebo, X. Qian, Q. Zhang, L. Chen, H. M. Cheng and W. Ren, Highly stable graphene-oxide-based membranes with superior permeability, *Nat. Commun.*, 2018, **9**, 1486.

2 Q. Xie, M. A. Alibakhshi, S. Jiao, Z. Xu, M. Hempel, J. Kong, H. G. Park and C. Duan, Fast water transport in graphene nanofluidic channels, *Nat. Nanotechnol.*, 2018, **13**, 238–245.

3 H. Huang, Z. Song, N. Wei, L. Shi, Y. Mao, Y. Ying, L. Sun, Z. Xu and X. Peng, Ultrafast viscous water flow through nanostrand-channelled graphene oxide membranes, *Nat. Commun.*, 2013, **4**, 2979.

4 J. Abraham, K. S. Vasu, C. D. Williams, K. Gopinadhan, Y. Su, C. T. Cherian, J. Dix, E. Prestat, S. J. Haigh, I. V. Grigorieva, P. Carbone, A. K. Geim and R. R. Nair, Tunable sieving of ions using graphene oxide membranes, *Nat. Nanotechnol.*, 2017, **12**, 546–550.

5 S. P. Surwade, S. N. Smirnov, I. V. Vlassiouk, R. R. Unocic, G. M. Veith, S. Dai and S. M. Mahurin, Water desalination using nanoporous single-layer graphene, *Nat. Nanotechnol.*, 2015, **10**, 459–464.

6 A. Morelos-Gomez, R. Cruz-Silva, H. Muramatsu, J. Ortiz-Medina, T. Araki, T. Fukuyo, S. Tejima, K. Takeuchi, T. Hayashi, M. Terrones and M. Endo, Effective NaCl and dye rejection of hybrid graphene oxide/graphene layered membranes, *Nat. Nanotechnol.*, 2017, **12**, 1083.

7 J. Li, X. Wang, G. Zhao, C. Chen, Z. Chai, A. Alsaedi, T. Hayat and X. Wang, Metal-organic framework-based materials: superior adsorbents for the capture of toxic and radioactive metal ions, *Chem. Soc. Rev.*, 2018, **47**, 2322–2356.

8 Z. Wang, S. Hu, J. Yang, A. Liang, Y. Li, Q. Zhuang and J. Gu, Nanoscale Zr-Based MOFs with Tailorable Size and Introduced Mesopore for Protein Delivery, *Adv. Funct. Mater.*, 2018, **28**, 1707356.

9 J. Wang, J. Tang, B. Ding, Z. Chang, X. Hao, T. Takei, N. Kobayashi, Y. Bando, X. Zhang and Y. Yamauchi, Self-Template-Directed Metal-Organic Frameworks Network and the Derived Honeycomb-Like Carbon Flakes via Confinement Pyrolysis, *Small*, 2018, **14**, 1704461.

10 C. Wang, Y. V. Kaneti, Y. Bando, J. Lin, C. Liu, J. Li and Y. Yamauchi, Metal–organic framework-derived one-dimensional porous or hollow carbon-based nanofibers for energy storage and conversion, *Mater. Horiz.*, 2018, **5**(3), 394–407.

11 B. Y. Guan, X. Y. Yu, H. B. Wu and X. W. D. Lou, Complex Nanostructures from Materials based on Metal-Organic Frameworks for Electrochemical Energy Storage and Conversion, *Adv. Mater.*, 2017, **29**(47), 1703614.

12 M. S. Yao, X. J. Lv, Z. H. Fu, W. H. Li, W. H. Deng, G. D. Wu and G. Xu, Layer-by-Layer Assembled Conductive MOF Nanofilms for Room Temperature Chemiresistive Sensing, *Angew. Chem., Int. Ed.*, 2017, **56**(52), 16510–16514.

13 A. Betard and R. A. Fischer, Metal-organic framework thin films: from fundamentals to applications, *Chem. Rev.*, 2012, **112**, 1055–1083.

14 T. Rodenas, I. Luz, G. Prieto, B. Seoane, H. Miro, A. Corma, F. Kapteijn, I. X. F. X. Llabres and J. Gascon, Metal-organic framework nanosheets in polymer composite materials for gas separation, *Nat. Mater.*, 2015, **14**, 48–55.

15 E. Jang, E. Kim, H. Kim, T. Lee, H.-J. Yeom, Y.-W. Kim and J. Choi, Formation of ZIF-8 membranes inside porous supports for improving both their H_2/CO_2 separation

performance and thermal/mechanical stability, *J. Membr. Sci.*, 2017, **540**, 430–439.

16 M. Yu, H. H. Funke, R. D. Noble and J. L. Falconer, H_2 separation using defect-free, inorganic composite membranes, *J. Am. Chem. Soc.*, 2011, **133**, 1748–1750.

17 C. Wang, X. Liu, N. Keser Demir, J. P. Chen and K. Li, Applications of water stable metal-organic frameworks, *Chem. Soc. Rev.*, 2016, **45**, 5107–5134.

18 J. G. Nguyen and S. M. Cohen, Moisture-Resistant and Superhydrophobic Metal−Organic Frameworks Obtained via Postsynthetic Modification, *J. Am. Chem. Soc.*, 2010, **132**, 4560–4561.

19 R. Chen, J. Yao, Q. Gu, S. Smeets, C. Baerlocher, H. Gu, D. Zhu, W. Morris, O. M. Yaghi and H. Wang, A two-dimensional zeolitic imidazolate framework with a cushion-shaped cavity for CO_2 adsorption, *Chem. Commun.*, 2013, **49**, 9500–9502.

20 Q. Liu, Z.-X. Low, Y. Feng, S. Leong, Z. Zhong, J. Yao, K. Hapgood and H. Wang, Direct conversion of two-dimensional ZIF-L film to porous ZnO nano-sheet film and its performance as photoanode in dye-sensitized solar cell, *Microporous Mesoporous Mater.*, 2014, **194**, 1–7.

21 Z. Zhong, J. Yao, Z.-X. Low, R. Chen, M. He and H. Wang, Carbon composite membrane derived from a two-dimensional zeolitic imidazolate framework and its gas separation properties, *Carbon*, 2014, **72**, 242–249.

22 Z. Zhong, J. Yao, R. Chen, Z. Low, M. He, J. Z. Liu and H. Wang, Oriented two-dimensional zeolitic imidazolate framework-L membranes and their gas permeation properties, *J. Mater. Chem. A*, 2015, **3**, 15715–15722.

23 T. Wang, Z. Kou, S. Mu, J. Liu, D. He, I. S. Amiinu, W. Meng, K. Zhou, Z. Luo, S. Chaemchuen and F. Verpoort, 2D Dual-Metal Zeolitic-Imidazolate-Framework-(ZIF)-Derived Bifunctional Air Electrodes with Ultrahigh Electrochemical Properties for Rechargeable Zinc-Air Batteries, *Adv. Funct. Mater.*, 2017, **28**(5), 1705048.

24 C. Guan, X. Liu, W. Ren, X. Li, C. Cheng and J. Wang, Rational Design of Metal-Organic Framework Derived Hollow $NiCo_2O_4$ Arrays for Flexible Supercapacitor and Electrocatalysis, *Adv. Energy Mater.*, 2017, **7**, 1602391.

25 C. Guan, A. Sumboja, H. Wu, W. Ren, X. Liu, H. Zhang, Z. Liu, C. Cheng, S. J. Pennycook and J. Wang, Hollow Co3O4 Nanosphere Embedded in Carbon Arrays for Stable and Flexible Solid-State Zinc-Air Batteries, *Adv. Mater.*, 2017, **29**(44), 1704117.

26 X. Liu, C. Guan, Y. Hu, L. Zhang, A. M. Elshahawy and J. Wang, 2D Metal-Organic Frameworks Derived Nanocarbon Arrays for Substrate Enhancement in Flexible Supercapacitors, *Small*, 2017, 1702641.

27 Z.-X. Low, A. Razmjou, K. Wang, S. Gray, M. Duke and H. Wang, Effect of addition of two-dimensional ZIF-L nanoflakes on the properties of polyethersulfone ultrafiltration membrane, *J. Membr. Sci.*, 2014, **460**, 9–17.

28 G. Liu, Z. Jiang, K. Cao, S. Nair, X. Cheng, J. Zhao, H. Gomaa, H. Wu and F. Pan, Pervaporation performance comparison of hybrid membranes filled with two-dimensional ZIF-L

nanosheets and zero-dimensional ZIF-8 nanoparticles, *J. Membr. Sci.*, 2017, **523**, 185–196.

29 W. T. Koo, J. S. Jang, S. Qiao, W. Hwang, G. Jha, R. M. Penner and I. D. Kim, Hierarchical Metal-Organic Framework-Assembled Membrane Filter for Efficient Removal of Particulate Matter, *ACS Appl. Mater. Interfaces*, 2018, **10**, 19957–19963.

30 H. Ting, H.-Y. Chi, C. H. Lam, K.-Y. Chan and D.-Y. Kang, High-permeance metal–organic framework-based membrane adsorber for the removal of dye molecules in aqueous phase, *Environ. Sci.: Nano*, 2017, **4**, 2205–2214.

31 A. Zirehpour, A. Rahimpour, A. Arabi Shamsabadi, M. Sharifian Gh and M. Soroush, Mitigation of Thin-Film Composite Membrane Biofouling via Immobilizing Nano-Sized Biocidal Reservoirs in the Membrane Active Layer, *Environ. Sci. Technol.*, 2017, **51**, 5511–5522.

32 K. Martin-Betancor, S. Aguado, I. Rodea-Palomares, M. Tamayo-Belda, F. Leganes, R. Rosal and F. Fernandez-Pinas, Co, Zn and Ag-MOFs evaluation as biocidal materials towards photosynthetic organisms, *Sci. Total Environ.*, 2017, **595**, 547–555.

33 X. Chen, Y. Zhang, J. Tang, M. Qiu, K. Fu and Y. Fan, Novel pore size tuning method for the fabrication of ceramic multi-channel nanofiltration membrane, *J. Membr. Sci.*, 2018, **552**, 77–85.

34 X. Li, Z. Li, L. Lu, L. Huang, L. Xiang, J. Shen, S. Liu and D. R. Xiao, The Solvent Induced Inter-Dimensional Phase Transformations of Cobalt Zeolitic-Imidazolate Frameworks, *Chem.–Eur. J.*, 2017, **23**, 10638–10643.

35 Y. Zhang, H. Chen, C. Guan, Y. Wu, C. Yang, Z. Shen and Q. Zou, Energy-Saving Synthesis of MOF-Derived Hierarchical and Hollow Co(VO$_3$)$_2$-Co(OH)$_2$ Composite Leaf Arrays for Supercapacitor Electrode Materials, *ACS Appl. Mater. Interfaces*, 2018, **10**, 18440–18444.

36 A. Huang, Q. Liu, N. Wang, Y. Zhu and J. Caro, Bicontinuous zeolitic imidazolate framework ZIF-8@GO membrane with enhanced hydrogen selectivity, *J. Am. Chem. Soc.*, 2014, **136**, 14686–14689.

37 B. Ding, X. Wang, Y. Xu, S. Feng, Y. Ding, Y. Pan, W. Xu and H. Wang, Hydrothermal preparation of hierarchical ZIF-L nanostructures for enhanced CO$_2$ capture, *J. Colloid Interface Sci.*, 2018, **519**, 38–43.

38 J. Zhang, T. Zhang, D. Yu, K. Xiao and Y. Hong, Transition from ZIF-L-Co to ZIF-67: a new insight into the structural evolution of zeolitic imidazolate frameworks (ZIFs) in aqueous systems, *CrystEngComm*, 2015, **17**, 8212–8215.

39 Z.-X. Low, J. Yao, Q. Liu, M. He, Z. Wang, A. K. Suresh, J. Bellare and H. Wang, Crystal Transformation in Zeolitic-Imidazolate Framework, *Cryst. Growth Des.*, 2014, **14**, 6589–6598.

40 B. Motevalli, N. Taherifar, H. Wang and J. Z. Liu, Ab Initio Simulations To Understand the Leaf-Shape Crystal Morphology of ZIF-L with Two-Dimensional Layered Network, *J. Phys. Chem. C*, 2017, **121**, 2221–2227.

41 H. T. Kwon, H. K. Jeong, A. S. Lee, H. S. An and J. S. Lee, Heteroepitaxially grown zeolitic imidazolate framework membranes with unprecedented propylene/propane

42 D.-Y. Kim, B. N. Joshi, J.-G. Lee, J.-H. Lee, J. S. Lee, Y. K. Hwang, J.-S. Chang, S. Al-Deyab, J.-C. Tan and S. S. Yoon, Supersonic cold spraying for zeolitic metal–organic framework films, *Chem. Eng. J.*, 2016, **295**, 49–56.

43 P. Jensen, S. R. Batten, G. D. Fallon, B. Moubaraki, K. S. Murray and D. J. Price, Structural isomers of M(dca)2 molecule-based magnets. Crystal structure of tetrahedrally coordinated sheet-like β-Zn(dca)2 and β-Co/Zn(dca)2, and the octahedrally coordinated rutile-like α-Co(dca)2, where dca− = dicyanamide, N(CN)2−, and magnetism of β-Co(dca)2, *Chem. Commun.*, 1999, (2), 177–178.

44 Z. Song, F. Qiu, E. W. Zaia, Z. Wang, M. Kunz, J. Guo, M. Brady, B. Mi and J. J. Urban, Dual-Channel, Molecular-Sieving Core/Shell ZIF@MOF Architectures as Engineered Fillers in Hybrid Membranes for Highly Selective CO$_2$ Separation, *Nano Lett.*, 2017, **17**, 6752–6758.

45 W. C. Lee, H. T. Chien, Y. Lo, H. C. Chiu, T. P. Wang and D. Y. Kang, Synthesis of Zeolitic Imidazolate Framework Core-Shell Nanosheets Using Zinc-Imidazole Pseudopolymorphs, *ACS Appl. Mater. Interfaces*, 2015, **7**, 18353–18361.

46 Y. Lo and D.-Y. Kang, Pseudopolymorphic seeding for the rational synthesis of hybrid membranes with a zeolitic imidazolate framework for enhanced molecular separation performance, *J. Mater. Chem. A*, 2016, **4**, 4172–4179.

47 Y. Gu, Y. N. Wu, L. Li, W. Chen, F. Li and S. Kitagawa, Controllable Modular Growth of Hierarchical MOF-on-MOF Architectures, *Angew. Chem., Int. Ed.*, 2017, **129**(49), 15864–15868.

48 L. Huang, S. Lau, H. Yang, E. Leong, S. Yu and S. Prawer, Stable superhydrophobic surface via carbon nanotubes coated with a ZnO thin film, *J. Phys. Chem. B*, 2005, **109**, 7746–7748.

49 X. Zhang, Y. Zhao, S. Mu, C. Jiang, M. Song, Q. Fang, M. Xue, S. Qiu and B. Chen, UiO-66-Coated Mesh Membrane with Underwater Superoleophobicity for High-Efficiency Oil-Water Separation, *ACS Appl. Mater. Interfaces*, 2018, **10**, 17301–17308.

50 S. L. Low, S. L. Ong and H. Y. Ng, Characterization of membrane fouling in submerged ceramic membrane photobioreactors fed with effluent from membrane bioreactors, *Chem. Eng. J.*, 2016, **290**, 91–102.

51 J. Wang, Y. Wang, Y. Zhang, A. Uliana, J. Zhu, J. Liu and B. Van der Bruggen, Zeolitic Imidazolate Framework/Graphene Oxide Hybrid Nanosheets Functionalized Thin Film Nanocomposite Membrane for Enhanced Antimicrobial Performance, *ACS Appl. Mater. Interfaces*, 2016, **8**, 25508–25519.

52 Y. Yuan and Y. Zhang, Enhanced biomimic bactericidal surfaces by coating with positively-charged ZIF nano-dagger arrays, *Nanomedicine*, 2017, **13**, 2199–2207.

53 Y.-L. Li, H.-Y. Chi, M.-Y. Kan, S.-Y. Pao, Y.-H. Kang, J.-J. Chen and D.-Y. Kang, Surface Engineering Layered Metal-Organic Framework to Enhance Processability and Stability in Water, *ChemNanoMat*, 2017, **3**, 902–908.